

This discussion paper is/has been under review for the journal The Cryosphere (TC).  
Please refer to the corresponding final paper in TC if available.

# Influence of anisotropy on velocity and age distribution at Scharffenbergbotnen blue ice area

T. Zwinger<sup>1</sup>, M. Schäfer<sup>2</sup>, C. Martín<sup>3</sup>, and J. C. Moore<sup>2,4,5</sup>

<sup>1</sup>CSC-IT Center for Science Ltd., Espoo, Finland

<sup>2</sup>Arctic Centre, University of Lapland, Rovaniemi, Finland

<sup>3</sup>British Antarctic Survey, Cambridge, UK

<sup>4</sup>College of Global Change and Earth System Science, Beijing Normal University, Beijing, China

<sup>5</sup>Department of Earth Sciences, Program for Air, Water and Landscape Sciences, Uppsala University, Uppsala, Sweden

Received: 29 April 2013 – Accepted: 21 May 2013 – Published: 25 June 2013

Correspondence to: T. Zwinger (zwinger@csc.fi)

Published by Copernicus Publications on behalf of the European Geosciences Union.

Title Page

Abstract

Introduction

Conclusions

References

Tables

Figures

◀

▶

◀

▶

Back

Close

Full Screen / Esc

Printer-friendly Version

Interactive Discussion



## Abstract

We use a full-Stokes thermo-mechanically coupled ice-flow model to study the dynamics of the glacier inside Scharffenbergbotnen valley, Dronning Maud Land, Antarctica. The domain encompasses a high accumulation rate region and, downstream a sublimation-dominated bare ice ablation area. The ablation ice area is notable for having old ice at its surface since the vertical velocity is upwards, and horizontal velocities are almost stagnant there. We compare the model simulation with field observations of velocities and the age distribution of the surface ice. A satisfactory match with simulations using an isotropic flow law was not found because of too high horizontal velocities and too slow vertical ones. However, the existence of a pronounced ice fabric may explain the present day surface velocity distribution in the inner Scharffenbergbotnen blue ice area. Near absence of data on the temporal evolution of Scharffenbergbotnen since the Late Glacial Maximum necessitates exploration of the impact of anisotropy using prescribed ice fabrics: isotropic, single maximum, and linear variation with depth, in both two-dimensional and three dimensional flow models. The realistic velocity field simulated with a non-collinear orthotropic flow law, however produced surface ages in significant disagreement with the few reliable age measurements and suggests that the age field is not in a steady state and that the present distribution is a result of a flow reorganization at about 15 000 yr BP. In order to fully understand the surface age distribution a transient simulation starting from the Late Glacial Maximum including the correct initial conditions for geometry, age, fabric and temperature distribution would be needed. It is the first time that the importance of anisotropy has been demonstrated in the ice dynamics of a blue ice area. This is useful to understand ice flow in order to better interpret archives of ancient ice for paleoclimate research.

## Scharffenbergbotnen blue ice area

T. Zwinger et al.

Title Page

Abstract

Introduction

Conclusions

References

Tables

Figures

◀

▶

◀

▶

Back

Close

Full Screen / Esc

Printer-friendly Version

Interactive Discussion



# 1 Introduction

Blue ice areas (BIAs) make up about 1 % of the surface area of Antarctica (Bintanja, 1999). They are usually formed where removal of snow fall by wind exceeds precipitation (Crary and Wilson, 1961), though low lying regions allow surface melt to be the dominant process. The Scharffenbergbotnen BIA, in common with most BIAs, is located in a region where wind speeds are higher than normal for Antarctica. High winds are in general because of steep gradients promoting katabatic flows, or in mountain areas where local wind fields determined by the geometry of mountains and ice surface lead to accelerated flow (Takahashi et al., 1992). Ice flow then brings deeper ice to the surface exposing aged solid blue ice (Whillans and Cassidy, 1983; Naruse and Hashimoto, 1982; Azuma et al., 1985; Bintanja, 1999). The with respect to snow-covered areas lowered surface albedo of BIAs enhances the effect of ablation above such areas (Bintanja and Reijmer, 2001). Consequently, isochrones are inclined relative to the surface – from sub-horizontal near the equilibrium line to near vertical at the stagnant ends of the valley (Naruse and Hashimoto, 1982; Whillans and Cassidy, 1983). This makes BIAs an ideal location to obtain “horizontal ice cores” – that is collecting samples for analysis along a shallow surface trench rather than traditional deep drilling – which may contain a record of climate record spanning the Holocene and perhaps longer (Moore et al., 2006; Sinisalo and Moore, 2010). Presently, however the problems in dating and interpreting climate records from horizontal ice cores have largely precluded their usefulness as climate archives (Sinisalo and Moore, 2010). Chief among these difficulties is an understanding of the long term stability of the blue ice as the surrounding ice sheet changes through a glacial cycle.

Ice sheet elevation changes at the glacial termination are likely to have been most pronounced in the nunatak areas, such as Scharffenbergbotnen, a few hundred kilometres from the coast (Pattyn and Declerq, 1998), since this is the transitional area between cold-based and warm-based ice flow. The surface of the major part of the East Antarctic plateau ice sheet may have been about 100 m lower in the last glacial

## Scharffenbergbotnen blue ice area

T. Zwinger et al.

Title Page

Abstract

Introduction

Conclusions

References

Tables

Figures



Back

Close

Full Screen / Esc

Printer-friendly Version

Interactive Discussion



than at present (Ritz et al., 2001; Pattyn, 1999; Jouzel et al., 1989). In contrast, the surface elevation at the margins of the plateau, may have been hundreds of meters higher (Näslund et al., 2000; Hättestrand and Johansen, 2005).

Understanding the present day ice dynamics of BIAs is challenging. Several attempts have been made using simplified flow models constrained by limited data (Naruse and Hashimoto, 1982; Azuma et al., 1985; Van Roijen, 1996; Grinsted et al., 2003; Sinisalo et al., 2004, 2007; Moore et al., 2006). However the complex geometry, usually including large ice thickness variations along the blue ice field, suggests that a three dimensional, higher order or full-Stokes model is needed to produce realistic ice flow simulations. Scharffenbergbotnen is the best studied BIA with a long history of observations including ice depth, surface velocities, mass balance, ice dating, ice temperature measurements, and both vertical and horizontal ice core archives of ice chemistry and water isotopes (the data sets are summarized in Sinisalo and Moore, 2010). Hence this BIA is a suitable test bed for numerical simulation using advanced flow modeling, which could provide insights on the dynamical evolution of the region since the last glacial.

After presenting the input data in Sect. 2, we introduce our model and the chosen initial and boundary conditions (Sect. 3). The simulation setup as well as the basic concepts of the applied anisotropic rheology follow in Sect. 4. The different approaches in terms of simulations are presented in Sect. 5, discussed in detail in Sect. 6, from which the conclusions (Sect. 7) with respect to the dynamics and age distribution at Scharffenbergbotnen are deduced.

## 2 Study area: Heimefrontfjella, Scharffenbergbotnen

Scharffenbergbotnen (SBB), north-west Sivorgfjella (74° S, 11° W, 1200 m a.s.l.), is a closed glaciated valley with inflow from the surrounding ice-sheet. The head of the valley acts as a dam on the main flow. There are two separate BIAs (light-gray in Fig. 1) in the valley, however this work focuses on the innermost one. Today, ice flows into the valley from north-western and western entrance and, to a very limited extent, over the

### Scharffenbergbotnen blue ice area

T. Zwinger et al.

Title Page

Abstract

Introduction

Conclusions

References

Tables

Figures

◀

▶

◀

▶

Back

Close

Full Screen / Esc

Printer-friendly Version

Interactive Discussion



## Scharffenbergbotnen blue ice area

T. Zwinger et al.

Title Page

Abstract

Introduction

Conclusions

References

Tables

Figures

◀

▶

◀

▶

Back

Close

Full Screen / Esc

Printer-friendly Version

Interactive Discussion



mountains in an ice-fall at the eastern end of the valley (close to stake 19 in Fig. 1). Geomorphological evidence (Hättstrand and Johansen, 2005) suggests that during the Late Glacial Maximum (LGM) the ice surface in the valley was 200–250 m higher than today, while the outside ice-sheet was only 50–150 m higher. The LGM ice sheet was able to overflow some of the passes along the valley walls and ice entered the valley from several more locations than today. As the elevation of the surrounding ice-sheet decreased after the LGM, the ice overflow became insignificant and the ice flow inside the valley decoupled from the main ice sheet flow.

A geological map of the Scharffenbergbotnen area is available from aerial photogrammetric surveys (1993, scale 1 : 25 000) as is a digital elevation model of the surface (100 m resolution) based on airborne surveys in 1985/86 over the whole Heimefrontfjella area (both ©Bundesamt für Kartographie und Geodäsie, Frankfurt am Main, <http://www.bkg.bund.de>). Ice thickness data (100 m resolution) comes from a radio-echo sounding campaign in 1987/88 and generally increases towards the center of the valley but with a maximum thickness of 1050 m at the north-western entrance (Herzfeld and Holmlund, 1990).

Several ice-cores have been drilled in the area that provide data on the age of the near-surface ice. A 52 m long vertical core was drilled in summer 1997/98 in the inner part of the valley (V in Fig. 1). The uppermost 45 m section has been dated to 10 500 (+700/–300) calendar years BP (van der Kemp et al., 2002), i.e. age calibrated for atmospheric  $^{14}\text{C}$  variations. A 100 m horizontal ice-core (the surface of the ice was sampled along a trench) was collected further upstreams in 2003/04 (at H in Fig. 1). The middle part of this ice core was dated to  $4426 \pm 215$  calendar years BP (Sinisalo and Moore, 2010). A longer horizontal core (2.7 km) was collected in 2006/07 (the complete slate-blue line in Fig. 1).

The age of the ice has been estimated at several locations (Table 1). The most reliable ages are from the  $^{14}\text{C}$  concentration in carbonaceous particles from ice core samples (Jenk et al., 2006), but only one location (Point H) has been dated (Sinisalo and Moore (2010), Table 1, Fig. 1). Other locations were sampled (including the band

## Scharffenbergbotnen blue ice area

T. Zwinger et al.

Title Page

Abstract

Introduction

Conclusions

References

Tables

Figures

◀

▶

◀

▶

Back

Close

Full Screen / Esc

Printer-friendly Version

Interactive Discussion



at the end of the flow line), but no other samples contained enough carbon to produce a reliable date. Van Roijen (1996) developed a method for dating blue ice by measuring  $^{14}\text{C}$  concentration in air trapped in the ice. In Van Roijen's method,  $^{14}\text{C}$  depth profiles in blue ice are translated into carbon ages with a correction made for  $^{14}\text{C}$  produced in situ, requiring an ice core to be analysed to about 50 m depth, and that results in the age at Point V, Table 1. Additional measurements are available from  $^{14}\text{C}$  analysis in 10 other locations, see Fig. 1 (numbered empty pentagons). These  $^{14}\text{C}$  ages had large uncertainties of up to several thousands of years (Van Roijen, 1996) since they were collected from shallow ice cores before the full impact of in situ  $^{14}\text{C}$  production was appreciated (van der Kemp et al., 2002). The results of the  $^{14}\text{C}$  measurements from the shallow ice cores (Van Roijen, 1996) have been corrected for atmospheric  $^{14}\text{C}$  variations and calibrated to calendar ages using OxCal, an online calibration tool (<http://c14.arch.ox.ac.uk>). The errors given in Table 1 correspond to the standard deviations given by the calibration. Since these measurements are much less reliable than the two measurements obtained at V and H, they are only used for approximate age estimation. In Sect. 5, discussions and comparisons with our model results are based mainly on the two most reliable datings.

In Sect. 5.2 we introduce a flow line model to reduce the full three dimensional solution complexity and to study principal influences from anisotropic rheology. The flow line was designed to coincide with the longer horizontal ice core (see Fig. 1). Inspection of aerial photos and maps, together with in-situ observations of the blue ice led to identification of a possible flow line on the valley. The main features used to identify this flow line were the visible bands on the ice surface (see e.g. Sinisalo and Moore (2010) – and several are also visible on the geological orthophoto map). We selected the route so that it passed through the apex of these curving structures as we supposed the ice velocity was fastest along those. The flow line upstream of the high accumulation area was chosen to follow the deepest surface incline path. The flow line terminated in the inner valley at a broad (3 m wide) band of dark colored ice that was about 1 m above the surrounding ice, and which we interpret as the confluence of the ice flow



measurements over shorter periods are consistent with the long term trend. Some results published in earlier articles have been improved upon here. Horizontal velocities are very small, the ice is hardly moving in this area compared with ice flow in the surrounding ice sheet. Over large areas of the BIA surface velocities are below  $1 \text{ myr}^{-1}$ .

5 The stake velocities are shown in Fig. 1 and Table 2. In addition we used some earlier measurements (Ber. Polarforsch. 86, 1991) surveyed using theodolites (see Fig. 1) within one single season that are less reliable than GPS surveys over longer periods.

### 3 Model

10 By the nature of its high viscosity, the flow of ice is described by the Stokes equation, which neglects inertia forces and sets the specific driving force, namely density times gravity,  $\rho\mathbf{g}$ , in balance with the divergence of the Cauchy stress,  $\text{div}\boldsymbol{\sigma}$ ,

$$\text{div}\boldsymbol{\sigma} + \rho\mathbf{g} = 0. \quad (1)$$

The Cauchy stress tensor,  $\boldsymbol{\sigma} = \boldsymbol{\tau} - \rho I$ , can be divided into the deviatoric stress,  $\boldsymbol{\tau}$ , and,  $\rho = -\text{tr}\boldsymbol{\sigma}/3$ , the isotropic pressure.

15 The standard way of treating ice in glaciers and ice sheets is to assume incompressibility, which is justified if the compression of firn has a negligible influence on the global dynamics of the system. Although in the high accumulation area between the two BIAs firn compaction could have an influence on the local dynamics, in the case of blue ice, where by definition we have no firn layer to account for, this certainly holds and the conservation of mass reduces to

$$\text{div}\mathbf{u} = \text{tr}\dot{\boldsymbol{\varepsilon}} = 0. \quad (2)$$

The strain rate tensor  $\dot{\boldsymbol{\varepsilon}}$  can be deduced from the velocity vector,  $\mathbf{u} = (u, v, w)$ , by

$$\dot{\boldsymbol{\varepsilon}} = \frac{1}{2} \left( \text{grad}\mathbf{u} + (\text{grad}\mathbf{u})^T \right). \quad (3)$$

If treated as an isotropic material, ice rheology is given by a Norton–Hoff power law, with the power law exponent  $n = 3$  in Eq. (5) known as Glen’s law in glaciology, which collinearly links the deviatoric stress  $\boldsymbol{\tau}$  with the strain-rate  $\dot{\boldsymbol{\epsilon}}$ :

$$\boldsymbol{\tau} = 2\eta\dot{\boldsymbol{\epsilon}}, \quad (4)$$

5 where the effective viscosity  $\eta$  is defined as

$$\eta = \frac{1}{2}(EA)^{-1/n}\dot{\epsilon}_e^{(1-n)/n}. \quad (5)$$

In Eq. (5),  $\dot{\epsilon}_e^2 = \text{tr}(\dot{\boldsymbol{\epsilon}}^2)/2$  is the square of the second invariant of the strain-rate. To a limited extent, the enhancement factor  $E$  can be used to mimic anisotropy effects (Ma et al., 2010).  $A = A(T')$  is a rheological parameter which depends on the ice temperature  $T'$  relative to the temperature melting point, via an Arrhenius law.

10 The temperature is obtained from the general balance equation of internal energy and reads

$$\rho c_v \left( \frac{\partial T}{\partial t} + \mathbf{u} \cdot \text{grad}T \right) = \text{div}(\kappa \text{grad}T) + \dot{\boldsymbol{\epsilon}} : \boldsymbol{\sigma}, \quad (6)$$

15 where  $\kappa = \kappa(T)$  and  $c_v = c_v(T)$  are the heat conductivity and specific heat of ice, respectively. The last term in the heat transfer equation represents the amount of energy produced by the viscous deformation, which because of the low shear rates in our application has no significant contribution and hence is neglected.

The complete set of equations is solved using the Finite Element Method (FEM) using the open source software package Elmer/Ice (Gagliardini et al., 2013; <http://elmerice.elmerfem.org>), which has already been applied to glacier simulations of different kinds (Zwinger et al., 2007; Zwinger and Moore, 2009; Zhao et al., 2013), and we use similar numerical settings as discussed in Martín and Gudmundsson (2012).

The age  $\Psi$  of the ice is governed by the advection equation

$$\frac{\partial \Psi}{\partial t} + u \frac{\partial \Psi}{\partial x} + w \frac{\partial \Psi}{\partial z} = 1. \quad (7)$$

Scharffenbergbotnen  
blue ice area

T. Zwinger et al.

Title Page

Abstract

Introduction

Conclusions

References

Tables

Figures

◀

▶

◀

▶

Back

Close

Full Screen / Esc

Printer-friendly Version

Interactive Discussion



Because of its purely advective nature, we chose to solve Eq. (7) using a semi-Lagrangian scheme integrated over a period of up to 15 000 yr using the steady state velocity field obtained with a thermo-mechanically coupled solution. Exactly the same semi-Lagrangian method was first applied and explained by Martín and Gudmundsson (2012). In Sect. 5 we chose to present results taken after 15 000 yr, as this corresponds with the timespan since the middle of the last deglaciation in Antarctica (EPICA community members, 2004).

### 3.1 Anisotropic rheology

Until recently, anisotropy in Elmer/Ice was restricted to the linear General Orthotropic Flow Law (GOLF Gillet-Chaulet et al., 2006) or a co-linear CAFFE model based on an anisotropic Flow Enhancement factor (Seddik et al., 2008, 2011). In more recent work (Martín et al., 2009; Ma et al., 2010), the orthotropic law has been extended to a non-linear form by adding an invariant in the anisotropic linear law. As we will show later, one of our main findings was the necessity to introduce anisotropic flow behavior to understand the ice dynamics of the Scharffenbergbotnen valley and match it qualitatively with the combined data of observed velocities, and surface age distributions. We did this by applying the model introduced and discussed in detail by Martín and Gudmundsson (2012). Then the non-covariant formulation of anisotropic flow Eq. (4) becomes a general tensor relation, which in index notation can be written as

$$\tau_{ij} = 2\eta_{ijkl}\dot{\epsilon}_{kl}. \quad (8)$$

The 36 independent components of the viscosity tensor  $\eta$  are functions of the polycrystalline fabric. Mathematically, this dependency is expressed in terms of the second and fourth order orientation tensors  $\mathbf{a}^{(2)}$  and  $\mathbf{a}^{(4)}$ , respectively, defined as

$$a_{ij}^{(2)} = \langle c_i c_j \rangle \text{ and } a_{ijkl}^{(4)} = \langle c_i c_j c_k c_l \rangle, \quad (9)$$

with  $\mathbf{c}$  being the c-axis unit vector and  $\langle \rangle$  the volume average. In order to express the fourth order tensor in terms of the second order tensor (Advani and Tucker, 1990), a closure relation is provided (Chung and Kwon, 2002; Gillet-Chaulet et al., 2006).

### 3.2 Boundary and initial conditions

5 The governing equations have to be accompanied by boundary conditions for the field variables. All our simulations are performed on a fixed geometry, reducing the otherwise transient kinematic free surface condition

$$\frac{\partial z_s}{\partial t} + u_s \frac{\partial z_s}{\partial x} + v_s \frac{\partial z_s}{\partial y} - w_s = a_s, \quad (10)$$

to

$$10 \quad \frac{\partial z_s}{\partial t} = 0, \quad (11)$$

and consequently rendering the surface net accumulation,  $a_s$ , to be part of the solution of the system rather than an additional boundary condition to it. By neglecting atmospheric pressure gradients and shear forces exerted by the atmosphere, the dynamic boundary condition at the free surface reduces to a vanishing Cauchy stress vector,

$$15 \quad \mathbf{t} = \boldsymbol{\sigma} \cdot \mathbf{n} = \mathbf{0}, \quad z = z_s(x, t), \quad (12)$$

where  $\mathbf{n}$  is the outward pointing surface normal,

$$\mathbf{n} = \left( -\frac{\partial z_s}{\partial x}, -\frac{\partial z_s}{\partial y}, 1 \right)^T / \left\| \left( -\frac{\partial z_s}{\partial x}, -\frac{\partial z_s}{\partial y}, 1 \right)^T \right\|. \quad (13)$$

The remaining variables to be set at the free surface are the mean average temperature – taken to be  $T_{z_s} = -20^\circ\text{C}$  – as well as the age of the downwards advected ice

$$20 \quad \Psi = 0, \quad z = z_s(x, t). \quad (14)$$

Title Page	
Abstract	Introduction
Conclusions	References
Tables	Figures
◀	▶
◀	▶
Back	Close
Full Screen / Esc	
Printer-friendly Version	
Interactive Discussion	



Because of the special hyperbolic nature of Eq. (7), this condition is set only if  $\mathbf{u} \cdot \mathbf{n} < 1$ . In other words, only if the velocity is pointing against the outward facing surface normal Eq. (13), do we set Eq. (14).

Even with the relatively large heat flux of  $q_{\text{geo}} = 60 \text{ mW m}^{-2}$  we used, only a minor area of the bedrock, beneath the deepest ice at the very outer end of the valley (where it has minor impact on the inner BIA dynamics), reaches pressure melting point. This allows for setting a freeze-on condition for the velocity, i.e.,  $\mathbf{u} = \mathbf{0}$ , all over this boundary. This, in consequence, prohibits a steady state solution of Eq. (7), as it would lead to infinite age,  $\Psi \rightarrow \infty$ , at the bedrock. As an initial condition for the age distribution,  $\Psi(\mathbf{x}, t = 0)$ , we assumed plug-flow and applied the analytic solution of Lliboutry (1979) using a constant artificial melt-rate of  $1.0 \times 10^{-6} \text{ myr}^{-1}$  to allow for steady state conditions to be applied.

#### 4 Simulation setup

The velocity field resulting from the Stokes equation is an instantaneous response to a given viscosity distribution and not directly influenced by temporal changes of the geometry. On the other hand, temperature and fabric evolution as well as the age/depth distribution depend on the flow history of the glacier and would demand a transient simulation starting from the LGM and extending to the present day. In particular, by our simulations it turned out that the age/depth distribution – even for fixed geometry – is not in a steady state and by the purely convective nature of Eq. (7) demands a transient approach even starting from before LGM to get the correct initial age/depth distribution. Such a simulation demands:

- the LGM geometry (initial condition for  $z_s$ ),
- the LGM age and fabric distribution,  $\Psi_{\text{LGM}}$  and  $a_{ij,\text{LGM}}^{(2)}$  (or spin-up simulation starting one glacier cycle earlier),

Title Page

Abstract

Introduction

Conclusions

References

Tables

Figures

◀

▶

◀

▶

Back

Close

Full Screen / Esc

Printer-friendly Version

Interactive Discussion



- the accumulation/ablation pattern during the whole simulation ( $a_s(\mathbf{x}, t)$  in Eq. 10),
- the surface temperature history from LGM to present  $T_s(\mathbf{x}_s, t)$ .

By the nature of the problem, at least the first of these items are largely undetermined. Additionally the computational effort required to run a full-Stokes model for such a long period, with relatively unconstrained geometrical evolution renders a prognostic simulation from LGM a highly unrealistic approach. Consequently, we focused our efforts on studying the effects of anisotropy on ice dynamics within the the fixed present day geometry assuming a steady thermal state and prescribed fabrics.

For all simulations we assume steady state ice-flow conditions and calculate the evolution of the age-distribution from a typical ice-sheet configuration to a blue-ice area. To that end, we calculate the steady-state temperature and flow distribution under the present conditions. Using the velocity solution from the steady state run, the age Eq. (7) is integrated from an initial vertically layered plug-flow distribution using a transient run, which – motivated by the values of the most reliable age measurements at the surface – starts at 15 kyr BP.

Based on the data sets presented in Sect. 2, a two-dimensional, unstructured footprint-mesh, covering the glaciated area of SBB in the horizontal plane was created using the open-source meshing software Gmsh (Geuzaine and Remacle, 2009). Horizontal resolution is 30 m in our main region of interest (close to the ice cores), 50 m in the rest of the valley and up to 100 m closer to the boundaries. We extruded this mesh in the vertical direction in 13 levels. The resulting mesh has about 61 000 nodes that are connected in 54 000 linear elements.

Elmer/Ice uses the Finite Element Method to discretize the governing equations. The resulting system matrices for the solution of the temperature field as well as the Stokes equation (velocities and pressure) is pre-conditioned with an incomplete LU decomposition and thereafter solved using the Generalized Conjugate Residual (GCR) method. Because of the non-linearities introduced by the material parameters (heat conductivity and capacity as well as viscosity) each solver for itself has to iteratively solve

**Scharffenbergbotnen  
blue ice area**

T. Zwinger et al.

Title Page	
Abstract	Introduction
Conclusions	References
Tables	Figures
◀	▶
◀	▶
Back	Close
Full Screen / Esc	
Printer-friendly Version	
Interactive Discussion	



a linearized system, obtained by a fixed-point iteration for resolving these nonlinearities. Due to their mutual coupling we also have to iteratively solve for temperature and the Stokes equation to obtain a converged solution for the steady state.

#### 4.1 Prescribed anisotropy

5 Three different setups were tested to study the principal influence of anisotropic rheology on the flow and the age/depth distribution:

(i) *Isotropic* flow using Glen's flow law.

(ii) A *depth-dependent*, piecewise linear *anisotropic* fabric distribution starting from isotropic and developing towards a single maximum fabric towards the bedrock, i.e.

$$10 \quad a_{11}^{(2)}(h, d) = a_{22}^{(2)}(h, d) = \max(1/3(1 - 2d/h), 0); \quad a_{33}^{(2)} = 1 - a_{11}^{(2)} - a_{22}^{(2)}, \quad (15)$$

with the local ice thickness  $h(x, y)$  and the vertical flow depth measured from the free surface,  $d$ .

(iii) An over the depth fixed *single maximum anisotropic* fabric:

$$15 \quad a_{11}^{(2)} = a_{22}^{(2)} = 0; \quad a_{33}^{(2)} = 1. \quad (16)$$

Note that Eq. (15) is defined for three-dimensions, and also applied for the flow-line model. The isotropic and the single maximum case define the extreme configurations of the fabric that may occur and comparison with measured values will show how pronounced the orientation of the c-axis is to be expected.

## 20 5 Results

This section presents the numerical simulations we conducted. First, we present the isotropic, three-dimensional (3-D) case, which leads to the problems of having too high

Title Page	
Abstract	Introduction
Conclusions	References
Tables	Figures
◀	▶
◀	▶
Back	Close
Full Screen / Esc	
Printer-friendly Version	
Interactive Discussion	



**Scharffenbergbotnen  
blue ice area**

T. Zwinger et al.

Title Page

Abstract

Introduction

Conclusions

References

Tables

Figures

◀

▶

◀

▶

Back

Close

Full Screen / Esc

Printer-friendly Version

Interactive Discussion



horizontal velocities in combination with a far too old ice at the measured ice core positions (see Sect. 2). We attempted to adjust the ice viscosity to produce a reasonable match to observations by globally tuning the enhancement factor,  $E$ , in relation (5) as well as changing the internal temperature distribution – and thereby the rate factor,  $A(T')$ , in Eq. (5). We did this by varying the surface temperature using the constraints given by climate history and the geothermal heat flux within realistic values. However, it was clear that we could not resolve the velocity and age issue. The most plausible remaining explanation for the mismatch of simulated and observed velocities is the *existence of a developed ice-fabric* that alters resistance to flow differently in horizontal and vertical direction. To get a more intuitive feeling for this impact, we employed a two-dimensional (2-D), but full stress component flow line model.

### 5.1 Simulations using isotropic rheology in 3-D

The first attempt to model the three-dimensional flow at SBB was to deploy the standard isotropic Glen's flow law (Paterson, 1994). As errors in the digital elevation model can strongly influence the steady state velocity field (Zwinger and Moore, 2009), a short prognostic run allowing for the free surface to adjust for these errors was made. Since no major adjustments of the free surface were observed we chose to use the unaltered geometry for the thermo-mechanically coupled steady state simulations. We use the resulting velocity field and the semi-Lagrangian method to integrate the age advection Eq. (7) over a time span of 15 kyr.

The result of this run is presented in Figs. 2 and 3. Comparing this with the measured velocities and ages (Fig. 1 and Table 2) it is immediately clear that simulated values of horizontal surface velocities exceed measured ones by almost one order of magnitude, and deviate considerably in direction in some places. Simultaneously, the simulated age distribution does not match the measured dates. They neither match the absolute values – they are far too old – nor in terms of the relative distribution – the gradient between the positions of the two most reliable measured values is much too large.

## 5.2 Simulations using 2-D flow line model

In order to reduce the complexity and the size of the problem, a two-dimensional flow-line model was set up. This approach was chosen to get a qualitative impression of the effect of imposing different fabrics on the glacier.

5 The results of all three setups are depicted in Figs. 4 and 5. The effect of both anisotropic fabric distributions are clearly visible. The *depth-dependent anisotropic* case (ii) does not tremendously alter the surface velocities – naturally, as at the surface we still have isotropic conditions, i.e.,  $a_{11} = a_{22} = a_{33} = 1/3$ . Deeper in the ice, the isochrones become much flatter, shortening the distance an ice particle has to travel  
10 from the accumulation area to the inner valley. For the inner BIA this results in a shifting of the old ice more towards the lower end of the valley and hence – at least qualitatively – improving the match with the observed age distribution. A similar effect occurs in the *single maximum anisotropic* case (iii), which, additionally, shows reduced horizontal velocities over the whole depth (Fig. 5), in particular at the free surface, where they  
15 now even underestimate the observed flow speeds in places.

## 5.3 Simulations using prescribed fabrics in 3-D

With the results from Sect. 5.2 in mind, we now turn back to the three-dimensional setup of SBB with the anisotropic distributions Eqs. (15) and (16), respectively. The results are depicted in Figs. 6 and 7.

20 The surface velocities in case (ii) with *depth-dependent anisotropic* fabric (Fig. 6a) are insignificantly different from the *isotropic* case (see Fig. 2). The issue of too high velocities (by an order of magnitude) with ill matching directions remains. Also the surface age distribution (Fig. 7a) resembles the one obtained with the *isotropic* flow law (see Fig. 3).

25 A clear change is observed with case (iii) the *single maximum anisotropic* fabric. The velocities (Fig. 6b) are greatly reduced with respect to the *isotropic* case and now match the directions, with absolute values slightly lower than observed magnitudes.

Title Page

Abstract

Introduction

Conclusions

References

Tables

Figures

◀

▶

◀

▶

Back

Close

Full Screen / Esc

Printer-friendly Version

Interactive Discussion



These slightly too slow velocities lead to almost stagnant ice at the lower end of the valley, resulting in too old ice ages there (Fig. 7b).

The change between the *isotropic/depth-dependent anisotropic* and the *single maximum anisotropic* case is even more clearly to be seen in the corresponding 3-D stream-lines. To that end we ran a stream-line solver (Runge–Kutta) provided within ParaView (Ahrens et al., 2005) backwards from a line at the surface that connects the sample-points H and V (see Fig. 1 and Table 1) in order to visualize the origin of ice particles that reach the surface in that region. The results of these post-processing steps are shown in Fig. 7. For the *isotropic* and *depth-dependent anisotropic* fabric cases, the origin of most particles is either from the region between the two BIAs areas or the southern flank on the other side of the surface moraine in the inner part of the valley (depicted in Fig. 1), which in itself already is a very unrealistic result (as stream-lines are not expected to cross surface moraines). This picture changes for the *single maximum anisotropic* fabric distribution, where all stream-lines are shifted to originate from areas close to the bedrock from within the outer part of the valley, more resembling the contours of our flow-line used for the initial studies. Another clear distinction between the two configurations is the integration time, i.e., the resulting physical time the Runge–Kutta method takes to trace a particle along the stream-line back to that particular position. Naturally, given the faster velocities, these computed times are much faster for the *isotropic/depth-dependent anisotropic* than the *single maximum anisotropic* fabric, with the latter quickly exceeding 50 000 yr once reaching the outer part of the valley.

## 6 Discussion

We presented simulations with an isotropic and two different ad-hoc prescribed fabric distributions: a depth-dependent distribution (evolving from isotropic at the surface to a vertical single maximum at one-third of the flow depth); and a uniform single vertical maximum fabric. The latter leads to a qualitatively correct reproduction of observed velocities at the BIA.

Title Page

Abstract

Introduction

Conclusions

References

Tables

Figures

◀

▶

◀

▶

Back

Close

Full Screen / Esc

Printer-friendly Version

Interactive Discussion



**Scharffenbergbotnen  
blue ice area**

T. Zwinger et al.

Title Page

Abstract

Introduction

Conclusions

References

Tables

Figures

◀

▶

◀

▶

Back

Close

Full Screen / Esc

Printer-friendly Version

Interactive Discussion



Since the anisotropic nature of ice introduces very strong differences in ice viscosity relative to the c-axis of the ice crystal, introducing anisotropic fabric provides a plausible solution to the need to reduce flow speed in horizontal directions and increase vertical ones. Other possible factors that would locally alter the ice viscosity, such as water content, ice impurities or damage tend to soften the ice (Paterson, 1994) and increase the velocity, and consequently cannot explain the deviation from modeled isotropic velocity with respect to the observed at SBB. Since the blue ice areas are unusual in that the annual layers are tilted (varying from sub-horizontal near the equilibrium line to near vertical at the closed end of the ablation area), the fabric evolves over time and space. The full evolution of the fabric would have to take into account the non-steady state evolution of the SBB valley since the LGM. During the LGM most of the valley was an accumulation region (Hättestrand and Johansen, 2005), and the blue ice was only formed as the surrounding ice sheet surface lowered and the mountain geometry created conditions suitable for effective removal of surface snow and firn (Malm, 2012).

We could not simulate such a dynamic evolution of the valley given the considerable uncertainty of the date and timing of the ice sheet change that then drives the blue ice area evolution, and of course such a long time prognostic run would be prohibitively expensive in computer resources. The flow line case suggested that both a depth varying fabric and a pure single maximum fabric would result in improvements to fit to observed velocities. In the three-dimensional simulation the depth-dependent fabric prescription (case (ii)) does not provide a satisfactory fit, while the single maximum prescription (case (iii)) performs much better (though with too low surface velocities). From the comparison of the 2-D (a–c) with the 3-D (d) results for the age and the velocity in Figs. 4–6, it becomes clear that due to the complexity of the flow field, a full 3-D simulation is needed to capture all features. This is confirmed by the twisted distribution of the streamlines depicted in Fig. 7.

It should be pointed out that there are some uncertainties in age observations, especially of ages in the valley. Some of the older measurements were made with a technique based on the  $^{14}\text{C}$  age of gas trapped in air, and this is known to be subject to

error caused by in-situ production of  $^{14}\text{C}$  by cosmic rays that penetrate surface ice layers (van der Kemp et al., 2002). Newer data come from measurements on particles that seem more reliable (Jenk et al., 2006), so there is relatively few data to constrain the model ages.

Our modeling results, in particular the difference between the prescribed depth-dependent and single-maximum fabric, suggest the presence of a strongly anisotropic ice-fabric in SBB not only towards the bottom of the ice column but also near the surface. Considering that the ice-fabric at a particular position not only depends on the local strain-rates but also on the history of previous strain-rates, our results indicate that the strongly anisotropic ice that typically appears in subsurface ice has been advected towards the surface of the BIA.

Strong fabric development has been observed in ice-cores close to the surface (Svensson et al., 2007). Radar studies also that show the presence of strong fabric development near the surface is widespread in Antarctica (Matsuoka et al., 2012). Recrystallization (polygonization), begins to work at depth and can both act to increase or reduce the strength of the fabric depending on the processes involved (Gagliardini et al., 2009). Even if ice was totally isotropic 15 kyr ago, flow-induced fabric can evolve rapidly (Martín et al., 2009) – that is in a fraction of the advection time-scale (thickness divided by vertical velocity). In our case that would be some fraction of tens of thousands of years. Hence it is reasonable to assume that strong fabric in SBB existed below the firn layer even before the LGM or the origin of the BIA. This could be tested by collection of samples in the blue ice field, however this has never been done at SBB. Indeed such measurements should be made if flow modeling is to be used to help interpret horizontal ice cores.

## 7 Conclusions

We investigated the ice dynamics of SBB using a full-Stokes flow model, as a tool to aid the interpretation of ice collected for paleoclimate research. We find that using

## Scharffenbergbotnen blue ice area

T. Zwinger et al.

Title Page

Abstract

Introduction

Conclusions

References

Tables

Figures

◀

▶

◀

▶

Back

Close

Full Screen / Esc

Printer-friendly Version

Interactive Discussion



**Scharffenbergbotnen  
blue ice area**

T. Zwinger et al.

Title Page

Abstract

Introduction

Conclusions

References

Tables

Figures

I◀

▶I

◀

▶

Back

Close

Full Screen / Esc

Printer-friendly Version

Interactive Discussion



standard isotropic ice fabric results in too high surface velocities and too low vertical ones, making a very poor match with observations of surface age and motion. While it is possible that non-linear evolution of the valley since the LGM may contribute to this discrepancy, the present day velocity field should be purely a function of the present day geometry and surface mass balance field. Attempts to vary viscosity using plausible ranges of geothermal heat flux and surface temperature changes since the LGM could not resolve this issue. All other reasons for a drastic change of the velocity field with respect to the isotropic rheology solution may be dismissed as implausible, hence the only remaining explanation for the observed velocities is the existence of pronounced anisotropic fabric.

We cannot provide a transient forcing of the free surface and the fabric evolution since the LGM, however we look at extreme configurations of the rheology for a fixed geometry in SBB. The best match with the observed velocity field was obtained with a fabric showing single vertical maximum. As anisotropy appears to be a key-factor in explaining the observed flow and age/depth distribution at SBB (and probably also in other blue ice areas), we suggest to investigate future ice samples not only with respect to chemistry, but also with respect to the orientation of fabric.

The remaining discrepancies concerning the match between the few reliable observed and computed ages at the surface certainly can be linked to the transient behaviour of the age/depth profile. Even with a fixed geometry and prescribed fabric and temperature distribution (which is equivalent to a given viscosity), no steady state of the age profile can be obtained, neither in 2-D nor 3-D simulations. Our simulated surface age in the inner part of the valley in any configuration is close to the integration time and the maximum observed age at the surface in the innermost blue ice area is about 15 ka. This suggests that the BIA was formed around that time which is plausible given the surface lowering that would have occurred in the ice sheet during the deglaciation.

This is the first time that the importance of anisotropy in the ice dynamics of a blue ice area has been assessed. We show that the understanding of ice anisotropy is key in order to decipher the paleoclimatic records of blue ice areas.

*Acknowledgements.* This work has been funded by the Finnish Academy (Suomen Akatemia) under the project *Dynamical evolution of Scharffenbergbotnen blue ice area since the Late Glacial Maximum*. We thank A. Grinsted (Centre for Ice and Climate, NBI, Univ. Copenhagen, Denmark) and A. Sinisalo (Univ. Oslo, Norway) for their insightful help on topics concerning their earlier work at SBB. We are grateful to C. H. Reijmer (Institute for Marine and Atmospheric research, Utrecht University, the Netherlands) for providing us with the data from AWS 7.

## References

- Advani, S. G. and Tucker, G. L.: Closure approximations for three-dimensional structure tensors, *J. Rheol.*, 34, 367–386, 1990. 3069
- Ahrens, J., Geveci, B., and Law, C.: ParaView: an end-user tool for large data visualization, in: *The Visualization Handbook*, edited by: Hansen, C. D., and Johnson, C. R., Elsevier, 2005. 3075
- Azuma, N., Nakawo, M., Higashi, A., and Nishio, F.: Flow pattern near Massif A in the Yamato bare ice field estimated from the structures and the mechanical properties of a shallow ice core, *Mem. NIPR*, 39, 173–183, 1985 3061, 3062
- Ber. Polarforsch. 86: Die Expedition ANTARKTIS-VIII mit FS “Polarstern” 1989/90, Bericht vom Fahrtabschnitt ANT-VIII/5, 1991 3066
- Bintanja, R.: On the glaciological, meteorological, and climatological significance of Antarctic blue ice areas, *Rev. Geophys.*, 37, 337–359, 1999. 3061
- Bintanja, R. and Reijmer, C. H.: Meteorological conditions over Antarctic blue-ice areas and their influence on the local surface mass balance, *J. Glaciol.*, 47, 37–50, 2001. 3061
- Chung, D. H. and Kwon, T. H.: Invariant-based optimal fitting closure approximation for the numerical prediction of flow-induced fiber orientation, *J. Rheol.*, 46, 169–194, 2002. 3069
- Crary, A. P. and Wilson, C. R.: Formation of “Blue” Glacier Ice by Horizontal Compressive Forces, *J. Glaciol.*, 3, 1045–1050, 1960. 3061
- EPICA community members: Eight glacial cycles from an Antarctic ice core, *Nature*, 429, 623–628, doi:10.1038/nature02599, 2004 3068
- Gagliardini, O., Gillet-Chaulet, F., and Montagnat, M.: A review of anisotropic polar ice models: from crystal to ice-sheet flow models, in: *Physics of Ice Core Records II*, Inst. of Low Temp. Sci., Hokkaido Univ, Sapporo, Japan, 149–166, 2009. 3077

## Scharffenbergbotnen blue ice area

T. Zwinger et al.

Title Page

Abstract

Introduction

Conclusions

References

Tables

Figures

◀

▶

◀

▶

Back

Close

Full Screen / Esc

Printer-friendly Version

Interactive Discussion



---

**Scharffenbergbotnen  
blue ice area**T. Zwinger et al.

---

[Title Page](#)[Abstract](#)[Introduction](#)[Conclusions](#)[References](#)[Tables](#)[Figures](#)[◀](#)[▶](#)[◀](#)[▶](#)[Back](#)[Close](#)[Full Screen / Esc](#)[Printer-friendly Version](#)[Interactive Discussion](#)

- Gagliardini, O., Zwinger, T., Gillet-Chaulet, F., Durand, G., Favier, L., de Fleurian, B., Greve, R., Malinen, M., Martín, C., Råback, P., Ruokolainen, J., Sacchetti, M., Schäfer, M., Seddik, H., and Thies, J.: Capabilities and performance of Elmer/Ice, a new generation ice-sheet model, *Geosci. Model Dev. Discuss.*, 6, 1689–1741, doi:10.5194/gmdd-6-1689-2013, 2013. 3067
- 5 Geuzaine, C. and Remacle, J.-F.: Gmsh: a three-dimensional finite element mesh generator with built-in pre- and post-processing facilities, *Int. J. Numer. Meth. Eng.*, 79, 1309–1331, 2009. 3071
- Gillet-Chaulet, F., Gagliardini, O., Meyssonier, J., Zwinger, T., and Ruokolainen, J.: Flow-induced anisotropy in polar ice and related ice-sheet flow modelling, *J. Non-Newton Fluid*, 124, 33–43, 2006. 3068, 3069
- 10 Grinsted, A., Moore, J., Spikes, V. B., and Sinisalo, A.: Dating Antarctic blue ice areas using a novel ice flow model, *Geophys. Res. Lett.*, 30, 2005, doi:10.1029/2003GL017957, 2003. 3062, 3065
- Herzfeld, U. C. and Holmlund, P.: Geostatistics in glaciology: implications of a study of Scharffenbergbotnen, Dronning Maud Land, East Antarctica, *Ann. Glaciol.*, 14, 107–110, 1990. 3063
- 15 Hättestrand, C. and Johansen, N.: Supraglacial moraines in Scharffenbergbotnen, Heimfrontjella, Dronning Maud Land, Antarctica – significance for reconstructing former blue ice areas, *Antarct. Sci.*, 17, 225–236, doi:10.1017/S0954102005002634, 2005. 3062, 3063, 3076
- 20 Jenk, T. M., Szidat, S., Schwikowski, M., Gäggeler, H. W., Brütsch, S., Wacker, L., Synal, H.-A., and Saurer, M.: Radiocarbon analysis in an Alpine ice core: record of anthropogenic and biogenic contributions to carbonaceous aerosols in the past (1650–1940), *Atmos. Chem. Phys.*, 6, 5381–5390, doi:10.5194/acp-6-5381-2006, 2006. 3063, 3077
- Jouzel, J., Raisbeck, G., Benoist, J. P., Yiou, F., Lorius, C., Raynaud, D., Petit, J. R., Barkov, N. I., Korotkevitch, Y. S., and Kotlyakov, V. M.: A comparison of deep Antarctic ice cores and their implications for climate between 65 000 and 15 000 years ago, *Quatern. Res.*, 31, 135–150, 1989. 3062
- 25 van der Kemp, W. J. M., Alderleisten, C., van der Borg, K., de Jong, A. F. M., Lamers, R. A. N., Oerlemans, J., Thomassen, M., and van de Wal, R. S. W.: In situ produced  $^{14}\text{C}$  by cosmic ray muons in ablating Antarctic ice, *Tellus B*, 54, 186–192, doi:10.1034/j.1600-0889.2002.00274.x, 2002. 3063, 3064, 3077
- 30 Lliboutry, L. A.: A critical review of analytical approximate solutions for steady state velocities and temperature in cold ice sheets, *Gletscherk. Glacialgeol.*, 15, 135–148, 1979. 3070

Scharffenbergbotnen  
blue ice area

T. Zwinger et al.

Title Page

Abstract

Introduction

Conclusions

References

Tables

Figures

◀

▶

◀

▶

Back

Close

Full Screen / Esc

Printer-friendly Version

Interactive Discussion



- Ma, Y., Gagliardini, O., Ritz, C., Gillet-Chaulet, F., Durand, G., and Montagnat, M.: Enhancement factors for grounded ice and ice shelves inferred from an anisotropic ice-flow model, *J. Glaciol.*, 56, 805–812, doi:10.3189/002214310794457209, 2010. 3067, 3068
- Malm, T.: Simulation of Wind Fields at Scharffenbergbotnen, Antarctica and their Impact on Blue Ice Areas, master thesis, Aalto University, School of Engineering, available at: <http://lib.tkk.fi/Dipl/2011/urn100517.pdf>, 2012. 3076
- Martín, C., Gudmundsson, G. H., Pritchard, H. D., and Gagliardini, O.: On the effects of anisotropic rheology on ice flow, internal structure, and the age–depth relationship at ice divides, *J. Geophys. Res.*, 114, F04001, doi:10.1029/2008JF001204, 2009. 3068, 3077
- Martín, C. and Gudmundsson, G. H.: Modelling of Kealey Ice Rise, Antarctica, reveals stable ice-flow conditions in East Ellsworth Land over millennia, submitted to *J. Glaciol.*, 2013. 3067, 3068
- Matsuoka, K., Power, D., Fujita, S., and Raymond, C. F.: Rapid development of anisotropic ice-crystal-alignment fabrics inferred from englacial radar polarimetry, central West Antarctica, *J. Geophys. Res.*, 117, F03029, doi:10.1029/2012JF002440, 2012. 3077
- Moore, J. C., Nishio, F., Fujita, S., Narita H., Pasteur E., Grinsted, A., Sinisalo, A., and Maeno, N.: Interpreting ancient ice in a shallow ice core from the South Yamato (Antarctica) blue ice area using flow modeling and compositional matching to deep ice cores, *J. Geophys. Res.*, 111, D16302, doi:10.1029/2005JD006343, 2006. 3061, 3062
- Naruse, R. and Hashimoto, M.: Internal flow lines in the ice sheet upstream of the Yamato Mountains, East Antarctica, *Mem. NIPR*, 24, 201–203, 1982. 3061, 3062
- Näslund, J. O., Fastook, J. L., and Holmlund, P.: Numerical modeling of the ice sheet in western Dronning Maud Land, East Antarctica: impacts of present, past and future climates, *J. Glaciol.*, 46, 54–66, 2000. 3062
- Paterson, W. S. B.: *The Physics of Glaciers*, 3 Edn., Pergamon, 1994. 3073, 3076
- Pattyn, F.: The variability of Antarctic ice-sheet response to the climatic signal, *Ann. Glaciol.*, 29, 273–278, 1999. 3062
- Pattyn, F. and Declair, H.: Ice dynamics near Antarctic marginal mountain ranges: implications for interpreting the glacial-geological evidence, *Ann. Glaciol.*, 27, 327–332, 1998. 3061
- Ritz, C., Rommelaere, V., and Dumas, C.: Modeling the evolution of Antarctic ice sheet over the last 420 000 years: implications for altitude changes in the Vostok region, *J. Geophys. Res.*, 106, 31943–31964, doi:10.1029/2001JD900232, 2001. 3062

Scharffenbergbotnen  
blue ice area

T. Zwinger et al.

Title Page

Abstract

Introduction

Conclusions

References

Tables

Figures

◀

▶

◀

▶

Back

Close

Full Screen / Esc

Printer-friendly Version

Interactive Discussion



Van Roijen, J. J.: Determination of ages and specific mass balances from C<sub>14</sub> measurements on Antarctic surface ice, Ph. D. thesis, Faculty of Physics and Astronomy, Utrecht University, Utrecht, the Netherlands, 1996. 3062, 3064

Seddik, H., Greve, R., Placidi, L., Hamann, I., and Gagliardini, O.: Application of a continuum-mechanical model for the flow of anisotropic polar ice to the EDML core, Antarctica, J. Glaciol., 54, 187, 631–664, doi:10.3189/002214308786570755, 2008. 3068

Seddik, H., Greve, R., Zwinger, T., and Placidi, L.: A full Stokes ice flow model for the vicinity of Dome Fuji, Antarctica, with induced anisotropy and fabric evolution, The Cryosphere, 5, 495–508, doi:10.5194/tc-5-495-2011, 2011. 3068

Shapiro, N. M. and Ritzwoller, M. H.: Inferring surface heat flux distributions guided by a global seismic model: particular application to Antarctica, Earth Planet. Sci. Lett., 223, 213–224, doi:10.1016/j.epsl.2004.04.011, 2004. 3065

Sinisalo, A. and Moore, J. C.: Antarctic blue ice areas – towards extracting palaeoclimate information, Antarc. Sci., 22, 99–115, doi:10.1017/S0954102009990691, 2010. 3061, 3062, 3063, 3064

Sinisalo, A., Grinsted, A., and Moore, J. C.: Dynamics of the Scharffenbergbotnen blue-ice area, Dronning Maud Land, Antarctica, Ann. Glaciol., 39, 417–423, 2004. 3062

Sinisalo, A., Grinsted, A., Moore, J. C., Meijer, H. A. J., Martma, T., and van de Wal, R. S. W.: Inferences from stable water isotopes on the Holocene evolution of Scharffenbergbotnen blue ice area, East Antarctica, J. Glaciol., 53, 427–434, 2007. 3062, 3065

Svensson, A., Durand, G., Mathiesen, J., Persson, A., and Dahl-Jensen, D.: Texture of the Upper 1000 m in the GRIP and North GRIP Ice Cores, in Physics of Ice Core Records II: Papers collected after the 2nd International Workshop on Physics of Ice Core Records, held in Sapporo, edited by: Hondoh, T., Japan, 2-6 February 2007, 2007. 3077

Takahashi, S., Endoh, T., Azuma, N., and Meshida, S.: Bare ice fields developed in the inland part of Antarctica, Proc. NIPR Symp. Polar Met. Glaciol., 5, 128–139, 1992. 3061

Whillans, I. M. and Cassidy, W. A.: Catch a falling star; meteorites and old ice, Science, 222, 55–57, 1983. 3061

Zhao, L., Tian, L., Zwinger, T., Ding, R., Zong, J., Ye, Q., and Moore, J. C.: Numerical simulations of Gurenhekou Glacier on the Tibetan Plateau using a full-Stokes ice dynamical model, The Cryosphere Discuss., 7, 145–173, doi:10.5194/tcd-7-145-2013, 2013. 3067

Zwinger T., Greve, R., Gagliardini, O., Shiraiwa, T., and Lyly, M.: A full Stokes-flow thermo-mechanical model for firn and ice applied to the Gorshkov crater glacier, Kamchatka, Ann. Glaciol., 45, 29–37, 2007. 3067

5 Zwinger, T. and Moore, J. C.: Diagnostic and prognostic simulations with a full Stokes model accounting for superimposed ice of Midtre Lovénbreen, Svalbard, The Cryosphere, 3, 217–229, doi:10.5194/tc-3-217-2009, 2009. 3067, 3073

Scharffenbergbotnen  
blue ice area

T. Zwinger et al.

Title Page

Abstract Introduction

Conclusions References

Tables Figures

◀ ▶

◀ ▶

Back Close

Full Screen / Esc

Printer-friendly Version

Interactive Discussion



Scharffenbergbotnen  
blue ice area

T. Zwinger et al.

**Table 1.** Measured calibrated ages at the surface including error bars and coordinate positions. The measured values except at V and H have large errors and can only be used as a guide to ages. Coordinates are given in UTM 29C.

site	age [yr]	error [yr]	Easting [m]	Northing [m]
b2	5978	2627	437 214.35	1 723 105.09
b3	4948	5405	436 537.15	1 723 307.14
b5	13 166	6883	438 183.76	1 722 806.78
b6	13 479	2842	439 395.07	1 722 064.31
b7	14 574	4390	438 708.77	1 722 806.66
b8	8264	1888	438 360.77	1 723 006.73
b10	12 119	8679	437 710.91	1 723 406.88
b14	2978	1063	436 262.64	1 724 953.09
b15	14 975	2884	438 925.77	1 722 656.62
b16	8084	1708	438 185.76	1 723 106.78
<b>V</b>	10 500	500	439 175.79	1 722 452.40
<b>H</b>	4426	215	438 432.31	1 723 013.61

Title Page

Abstract

Introduction

Conclusions

References

Tables

Figures

◀

▶

◀

▶

Back

Close

Full Screen / Esc

Printer-friendly Version

Interactive Discussion



**Table 2.** Measured surface velocities. Coordinates are in UTM 29 C.

site	Velocity [ $\text{m yr}^{-1}$ ]	Easting [m]	Northing [m]
S1	0.161	438 828.65	1 722 527.04
S2	0.358	437 876.72	1 722 897.62
S3	0.301	436 949.11	1 723 273.82
S4	0.241	436 018.18	1 723 635.99
S5	0.146	435 111.34	1 723 999.86
S6	0.124	434 203.94	1 724 379.20
e1183	0.174	434 087.58	1 723 023.08
Bi1	0.100	439 107.11	1 722 569.08
Bi4	0.142	438 917.10	1 722 672.78
Bi5	0.145	438 914.97	1 722 673.77
SF1	1.699	436 834.46	1 726 301.26
SF2	2.058	437 274.67	1 726 190.40
SF3	1.863	436 892.27	1 726 509.94
SF4	3.111	437 137.94	1 726 887.94
SF5	3.041	436 657.58	1 727 014.65
SF6	1.900	435 009.84	1 726 569.54
SF7	0.118	433 290.53	1 724 402.85
3	0.291	437 570.43	1 723 537.73
5	0.093	435 548.52	1 724 952.50
6	0.554	435 686.91	1 725 891.61
7	0.171	434 898.37	1 725 657.45
8	0.049	434 022.38	1 725 386.28
11	0.237	433 845.29	1 722 684.43
12	0.080	435 164.38	1 722 815.35
13	0.241	436 293.16	1 722 929.71
14	0.139	433 605.43	1 722 599.62
24	0.052	435 130.99	1 722 293.10
26	0.237	436 436.46	1 723 418.37
27	0.103	434 596.84	1 721 715.66

Title Page

Abstract

Introduction

Conclusions

References

Tables

Figures

◀

▶

◀

▶

Back

Close

Full Screen / Esc

Printer-friendly Version

Interactive Discussion





Scharffenbergbotnen  
blue ice area

T. Zwinger et al.

Title Page

Abstract

Introduction

Conclusions

References

Tables

Figures

◀

▶

◀

▶

Back

Close

Full Screen / Esc

Printer-friendly Version

Interactive Discussion

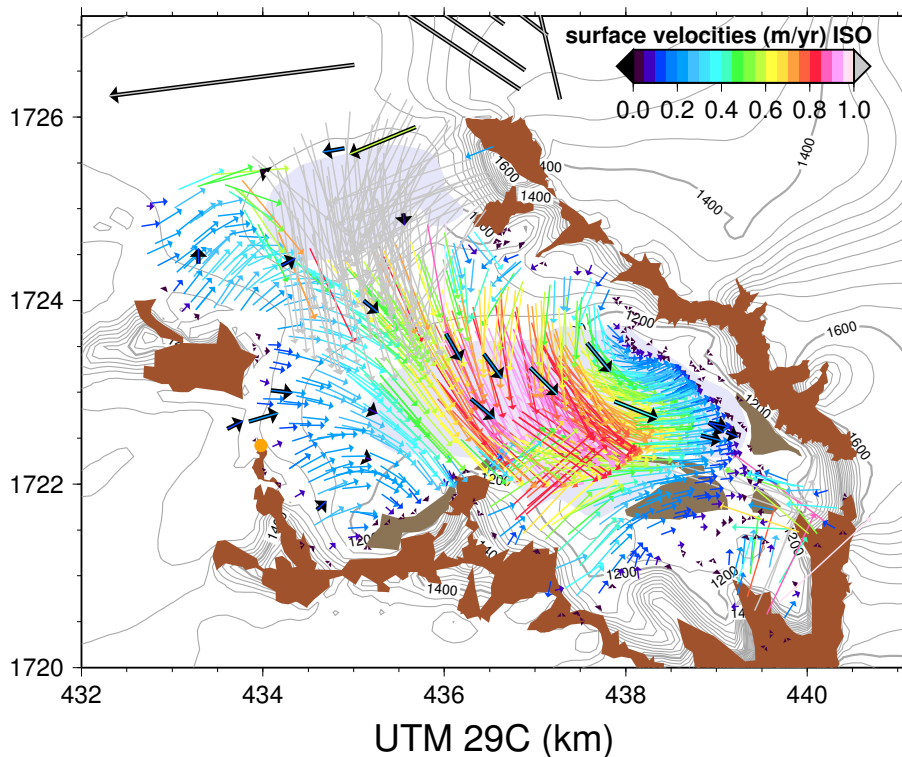


**Fig. 2.** Horizontal velocity distribution (scale bar) obtained with the isotropic Glen's flow law compared with measured velocities (thick arrows, see Table 2 for values). Discrepancies in both direction and magnitude (with observed velocities being almost an order of magnitude smaller) can be easily seen.

Scharffenbergbotnen  
blue ice area

T. Zwinger et al.

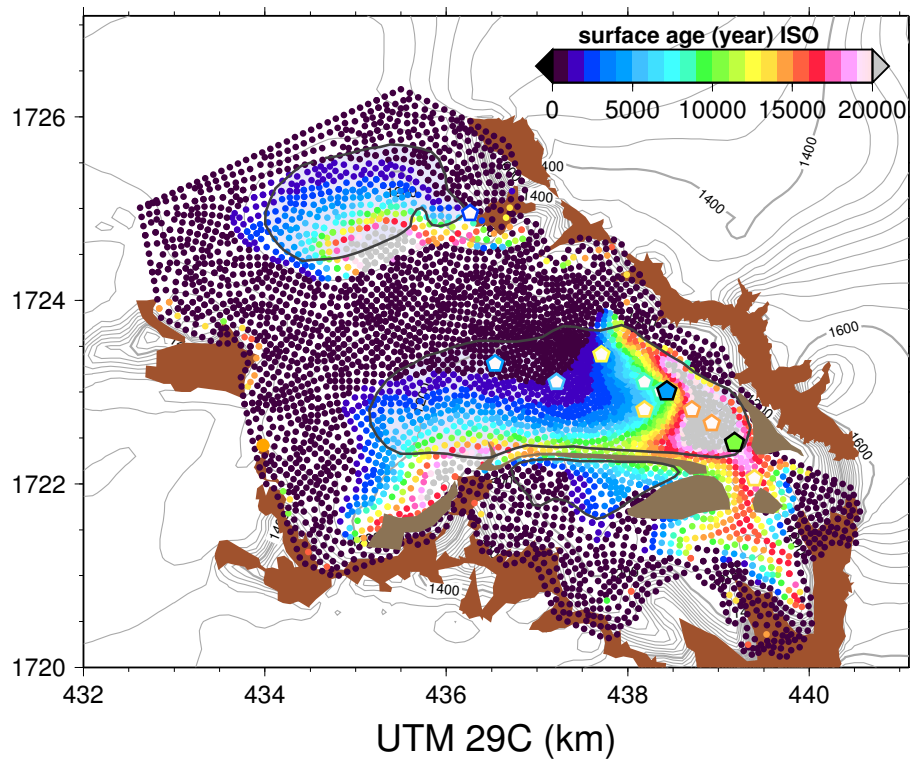


**Fig. 3.** Age (dots - scale bar) distribution obtained with the isotropic Glen's flow law and a 15 kyr integration of the age equation compared to measured (pentagons). Solid lines enclose BIAs.

Title Page

Abstract

Introduction

Conclusions

References

Tables

Figures

◀

▶

◀

▶

Back

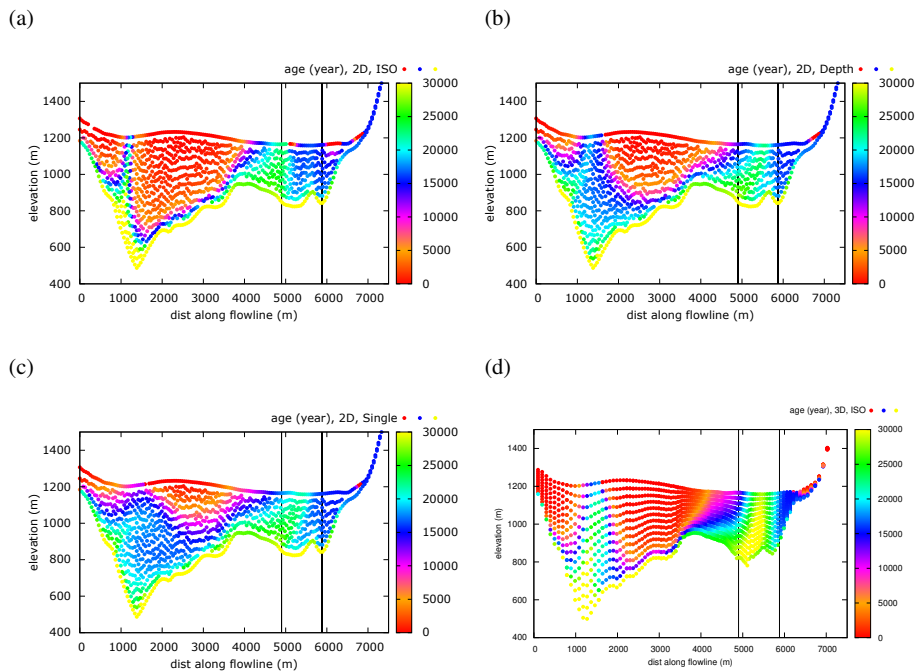
Close

Full Screen / Esc

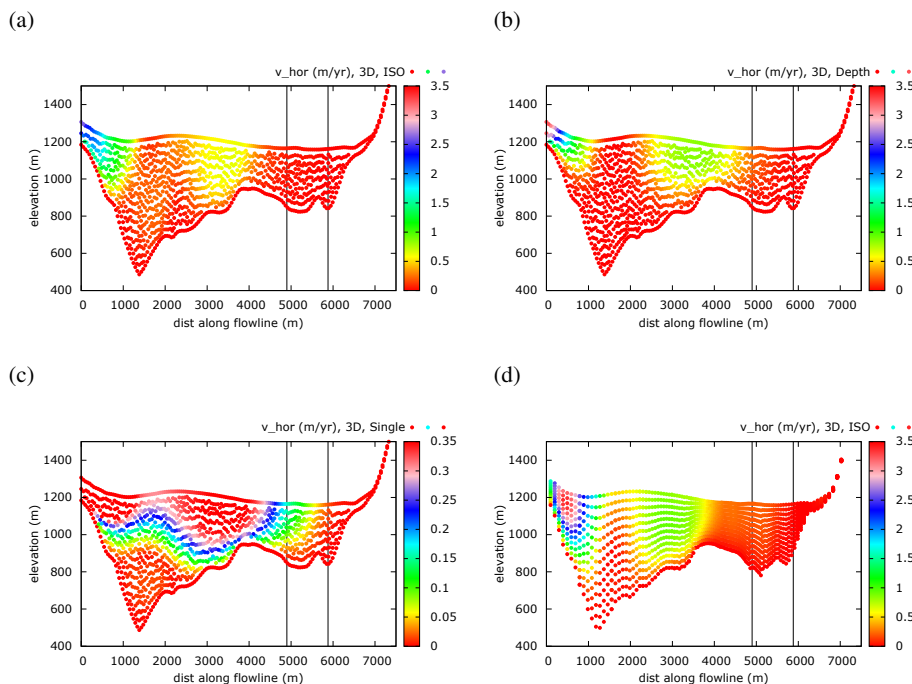
Printer-friendly Version

Interactive Discussion



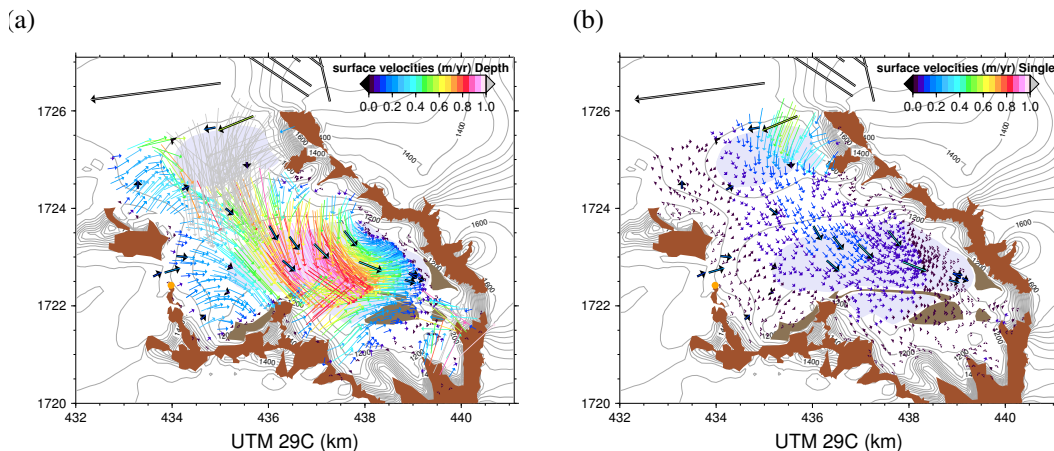
[Title Page](#)[Abstract](#)[Introduction](#)[Conclusions](#)[References](#)[Tables](#)[Figures](#)[◀](#)[▶](#)[◀](#)[▶](#)[Back](#)[Close](#)[Full Screen / Esc](#)[Printer-friendly Version](#)[Interactive Discussion](#)

**Fig. 4.** Comparison of age values obtained on the flow-line model using (a) isotropic Glen's flow law, (b) depth-dependent fabric and (c) single maximum fabric distribution for an integration over 15 kyr. In (d) we show a comparison with a section from the three-dimensional isotropic case (Fig. 3) along the flow-line shown in Fig. 1. The two vertical lines mark the intersection with the horizontal ice core at points V and H.



**Fig. 5.** Comparison of absolute velocity values obtained on the flow-line model using **(a)** isotropic Glen’s flow law, **(b)** depth-dependent fabric/depth and **(c)** single maximum fabric distribution (mind the different scale). In **(d)** we show a comparison with a section from the three-dimensional isotropic case (Fig. 2) along the flow-line shown in Fig. 1. It comes clear that in case of the single maximum fabric the velocities get one order of magnitude lower. The two vertical lines mark the intersection with the horizontal ice core at points V and H.

[Title Page](#)
[Abstract](#)
[Introduction](#)
[Conclusions](#)
[References](#)
[Tables](#)
[Figures](#)
[◀](#)
[▶](#)
[◀](#)
[▶](#)
[Back](#)
[Close](#)
[Full Screen / Esc](#)
[Printer-friendly Version](#)
[Interactive Discussion](#)

**Fig. 6.** Surface velocity (vectors) for the anisotropic flow law using (a) a depth-dependent fabric and (b) a single maximum fabric distribution. The surface velocities in the depth-dependent anisotropic case (a) are not significantly altered with respect to the isotropic case. However, applying a single maximum fabric reduces velocities (even reducing them too much) and produces better agreement in direction.

Title Page

Abstract

Introduction

Conclusions

References

Tables

Figures

◀

▶

◀

▶

Back

Close

Full Screen / Esc

Printer-friendly Version

Interactive Discussion



Scharffenbergbotnen  
blue ice area

T. Zwinger et al.

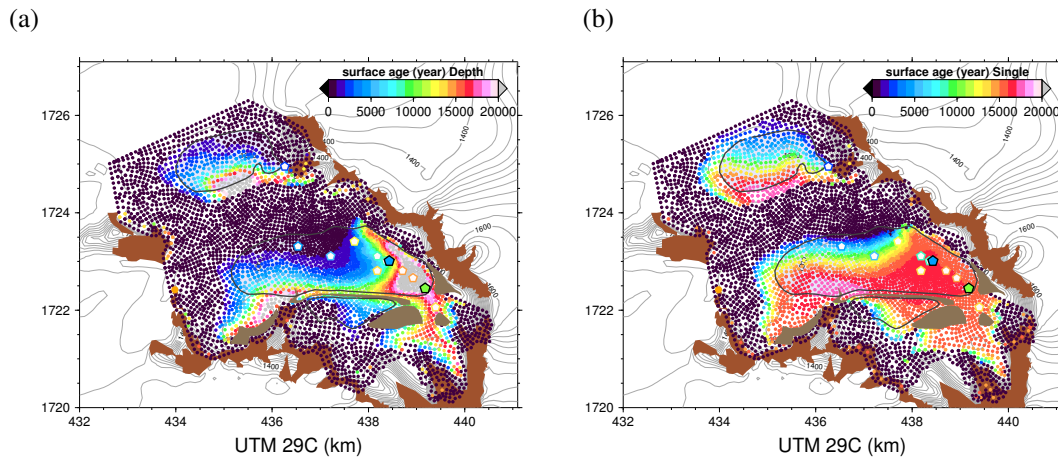


**Fig. 7.** Age (dots) distribution obtained with the anisotropic flow law using **(a)** depth-dependent fabric distribution and **(b)** single maximum fabric for integration times of 15 kyr.

Title Page

Abstract

Introduction

Conclusions

References

Tables

Figures

I◀

▶I

◀

▶

Back

Close

Full Screen / Esc

Printer-friendly Version

Interactive Discussion



Scharffenbergbotnen  
blue ice area

T. Zwinger et al.

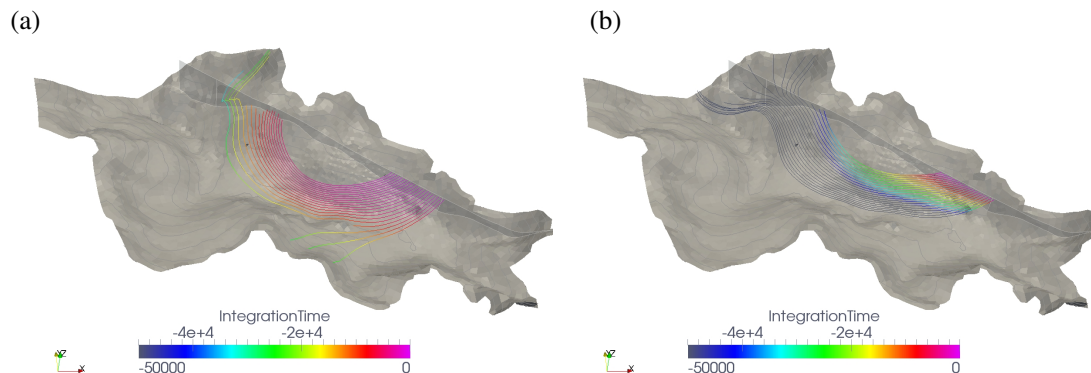


**Fig. 8.** Streamlines obtained with the backward Runge-Kutta method implemented in ParaView starting from the area where the ice cores have been sampled, colored by integration time given in years **(a)** isotropic and **(b)** single maximum fabric/depth distribution. The depth-dependent anisotropic fabric (not shown) is almost the same as the isotropic case and is characterized by stream-lines originating in the area between the inner and the outer BIA and at the southern flanks. In contrary, the single maximum fabric shifts the origin of the stream-lines towards the outer parts of the valley and significantly increases the travel time of the fluid particles.

[Title Page](#)[Abstract](#)[Introduction](#)[Conclusions](#)[References](#)[Tables](#)[Figures](#)[◀](#)[▶](#)[◀](#)[▶](#)[Back](#)[Close](#)[Full Screen / Esc](#)[Printer-friendly Version](#)[Interactive Discussion](#)